Hodograph Curvature and Updraft Intensity in Numerically Modeled Supercells

HAROLD E. BROOKS* AND ROBERT B. WILHELMSON

Department of Atmospheric Sciences, University of Illinois, Urbana, Illinois

16 September 1991 and 12 August 1992

ABSTRACT

A set of numerical simulations of supercell thunderstorms has been carried out with a range of low-level curvatures in the environmental hodograph and midlevel shears. They cover a range of hodograph "shape," as measured by the integrated helicity of the lowest 3 km of the hodograph. The peak updraft occurs in the first hour of the storms and tends to be greater for larger values of environmental helicity. There is also a slight tendency for greater updraft intensity with lesser values of midlevel shear. Significantly, air in the core of the updrafts at midlevels (~5 km) is not the most unstable air at the level. The most buoyant air rises in a region with a downward-directed pressure gradient force, which slows its ascent. Conversely, pressure gradient forces at lower levels (2–3 km) accelerate less buoyant air upward into the core of the midlevel updrafts. The pressure gradient force is larger in the cases with more curvature in the environmental wind than the low-curvature environments. This is consistent with predictions of the pressure gradient force derived from a simple Beltrami flow model of a rotating thunderstorm and a scale analysis.

1. Introduction

McCaul (1989, 1991) has described examples of supercell thunderstorms in environments characterized by low instability and large directional shear in low levels. A question that arises naturally from these observations is how strong updrafts can develop in environments with weak instability. McCaul (1989) showed that strong shear plays a crucial role in enhancing updrafts in these storms using the three-dimensional numerical cloud model of Klemp and Wilhelmson (1978). In this note, we will consider a larger set of simulations with a single moderately unstable thermodynamic profile in order to isolate the effects of curvature of the low-level hodograph on updraft growth. We also use a simple analytic model of rotating thunderstorm to evaluate the importance of curvature on maximum updraft strength.

A fundamental measure of the strength of a thunderstorm is the maximum intensity of the updraft within it. Parcel theory implies that the maximum updraft due to buoyancy effects is

$$w_b = \sqrt{2 \times \text{CAPE}}, \tag{1}$$

where CAPE is the convective available potential energy of the environment, given by

$$\text{CAPE} = g \int_{\text{LFC}}^{E_L} \frac{\theta_p - \theta_0}{\theta_0}\, dz, \tag{2}$$

where θ_0 is the potential temperature of the environment and θ_p is the potential temperature of the profile associated with a surface parcel raised along the moist adiabat from the level of free convection (LFC) to the equilibrium level (E_L). The application of (1) to thunderstorms implicitly assumes that the parcel with the maximum velocity at any level is associated with the highest buoyancy and that the work done by the pressure gradient force is negligible. Water loading and mixing, both physical and computational, will cause the actual maximum vertical velocity to be less than w_b.

In this note, we examine a relationship between the low-level environmental vertical wind shear and the early updraft strength in numerically simulated supercell thunderstorms. In particular, we find that model storms initialized in environments with high values of storm-relative integrated helicity have stronger updrafts from the early stages of the simulation than storms in low-helicity environments for the same thermodynamic conditions. Helicity, the inner product of the velocity and vorticity vectors of a flow integrated over a volume, provides a simple measure of the amount of curvature of the hodograph. Davies-Jones et al. (1990) compute the storm-relative helicity in the lowest 3 km of the environment using the formula

$$H(c) = -\int_0^h \mathbf{k} \cdot (\mathbf{V} - \mathbf{c}) \times \frac{d\mathbf{V}}{dz}\, dz, \tag{3}$$

where $\mathbf{V}$ is the environmental wind vector and $\mathbf{c}$ is the

* Current affiliation: NOAA/ERL National Severe Storms Laboratory, Norman, Oklahoma.

Corresponding author address: Dr. Harold E. Brooks, NOAA/NSSL, 1313 Halley Circle, Norman, OK 73069.

storm motion vector. This quantity can be interpreted geometrically as minus twice the signed area swept out by the storm-relative wind vector on a hodograph, so that H increases with increasing curvature of the hodograph. (The sign convention is such that the helicity is positive if the wind veers with height.) Davies-Jones et al. (1990) have shown that H has promise as a tool for the operational evaluation of the tornadic potential for an atmospheric environment. In this paper, we use it simply as a measure of the curvature of the hodograph.

In order to look at the updraft strength, we begin with the vertical equation of motion. Neglecting turbulence, it is

$$\frac{dw}{dt} = -c_p\theta_0 \frac{\partial \Pi'}{\partial z} + B, \tag{4}$$

where w is the vertical velocity, Π' is the perturbation from the base-state nondimensional pressure given by

$$\Pi = \left(\frac{p}{p_0}\right)^{R/c_p},$$

and B is the buoyancy given by

$$B = g\left(\frac{\theta'}{\theta_0} + 0.61q_v - [q_c + q_r]\right), \tag{5}$$

with g the acceleration due to gravity, θ' the perturbation potential temperature, and q_v, q_c, and q_r are the mixing ratios for water vapor, cloud water, and rainwater, respectively.

Previous numerical modeling studies (Weisman and Klemp 1984; McCaul 1989) have shown that the acceleration caused by the vertical pressure gradient term in (4) can be large. [Note that we have not divided the vertical pressure gradient term in (4) into contributions from separate dynamic and buoyancy effects, as was done by Weisman and Klemp (1984) and McCaul (1989).] This acceleration results from an interaction of the growing updraft with the environmental wind shear, as discussed by Rotunno and Klemp (1982). Rotunno and Klemp showed a stronger updraft in a supercell initialized with a curved hodograph compared to straight hodograph for a single case, and Weisman and Klemp (1984) ran a series of semicircular hodographs in which the updrafts became more intense with increasing radius of the hodograph. Beginning with those studies as a background, we will focus in particular on the contribution of the environmental hodograph curvature on the vertical pressure gradient. The two acceleration terms in (4) (pressure and buoyancy) will be evaluated along trajectories that end in the maximum updraft and maximum buoyancy locations at midlevels. The pressure gradient acts to reduce the updraft within air parcels rising to the maximum buoyancy location, while accelerating those rising to the maximum updraft location. Further, we will show that the vertical pressure gradient obtained from a simple model of a thunderstorm in a circular hodograph qualitatively supports the results shown by the numerical simulations. Our results indicate the importance of curvature of the hodograph, particularly in low levels, in intensifying updrafts. This effect is of relevance to the development of supercells in low-buoyancy environments.

2. Experimental design

The Klemp–Wilhelmson cloud model (Wilhelmson and Chen 1982) was used to carry out a set of simulations in a 70 km × 70 km × 16.3 km domain. The horizontal resolution was 1 km, and the vertical resolution varied with height as

$$Dz_k = 200[1 + 0.5 \tanh(k - 8)], \tag{6}$$

where Dz_k is the thickness of layer k in m. The result was that in the lowest 1.2 km the vertical resolution was 200 m, while at the top it was 600 m. The large and small time steps were 5 s and 0.833 s, respectively. The time-smoothing coefficients on both the large and small time steps were 0.1, while the vertical second-order and the horizontal fourth-order computational smoothing coefficients were 100 $m^2 s^{-1}$ and 2.5×10^8 $m^4 s^{-1}$. The Coriolis terms and surface drag were turned off. A warm bubble with a maximum temperature perturbation of 2 K was used to initiate all storms.

Twenty-one simulations were carried out, each with the same thermodynamic profile, to look at the effects of shear on supercell thunderstorm structure. The thermodynamic profile is shown in Fig. 1. It is similar to that used by Weisman and Klemp (1982, 1984), except with drier air at midlevels, and a gradient of moisture in the lowest kilometer. The surface water vapor mixing ratio is 15 g kg^{-1}. The CAPE associated with this sounding is approximately 2100 J kg^{-1}, equivalent to a maximum updraft of 64.8 m s^{-1}, according to parcel theory. Combinations of three midlevel wind profiles and seven low-level (below 3 km) wind profiles were used to form the 21 initial hodographs. The midlevel hodograph structure had constant rectilinear shear (straight hodograph segment) of 10^{-2} s^{-1} from 3 to 7 km, 5×10^{-3} s^{-1} from 3 to 7 km, and 5×10^{-3} s^{-1} from 3 to 11 km. Above the upper level, winds were held constant. This structure was combined with seven low-profiles, six with varying amounts of curvature and one with a continuation of the midlevel shear profile down to the surface. The curvature profiles were constructed by linearly increasing the wind speed and the change in wind direction from the ground to 3 km. The six low-level hodographs with curvature are shown in Fig. 2. Table 1 gives the amount of the change in wind speed and direction from the surface to 3 km for each of the profiles, as well as the bulk Richardson index (BRI) (Weisman and Klemp 1982, 1984) for the strong (10×10^{-3} s^{-1}) and

moderate (5×10^{-3} s^{-1}) midlevel shear profiles. BRI is given by

$$\text{BRI} = \frac{\text{CAPE}}{\frac{1}{2}S^2}, \qquad (7)$$

where S is the magnitude of the difference between the density-weighted mean wind over the lowest 500 m and the density-weighted mean wind over the lowest 6 km. Except for the storm in the strong rectilinear shear environment, the BRI varies only from 26.5 to 39.6, within the range associated with supercell development by Weisman and Klemp. All of the simulations produced supercell storms, with long-lasting rotating updrafts. The storms became supercells much more rapidly than those of Weisman and Klemp (1984), with the storms in the environments with curvature taking on distinctly supercellular characteristics by 25 minutes as illustrated by the correlation coefficient between vertical velocity and vertical vorticity within the updraft reaching 0.5. All of the updrafts except one (the strong rectilinear shear case) reached their peak intensity in the first hour. We will limit the analysis that follows to the intensity of the strong updraft in the early stages of each storm.

3. Results

In general, the simulated storms reach only 0.5–0.8 of w_b, as computed from (1). Figure 3 shows the vertical kinetic energy density associated with the maximum intensity of the updraft (which occurred before 3600 s, except for the strong rectilinear shear case, which did not reach its maximum until after 10 000 s) for each simulation ($w_{\max}^2/2$), plotted against the storm-relative helicity of the environment. The storm motion used to compute the environmental helicity is the average velocity between 1800 and 3000 s, except in the strong rectilinear shear case, for which the storm motion after 10 000 s is used. During this period, the storm motion is not constant, with each storm accelerating to the east, by up to 5 m s^{-2} for case A1. (The letter refers to the midlevel shear magnitude as in Table 1, with A corresponding to 10^{-2} s^{-1} from 3 to 7 km, B to 5×10^{-3} s^{-1} from 3 to 7 km, and C to 5×10^{-3} s^{-1} from 3 to 11 km. The numbers range from 1 to 6 as the helicity decreases.) This results in an increase in the helicity of no more than 100 m^2 s^{-2} as the storm accelerates for the large-curvature, high-helicity hodographs, with the change being less for the hodographs with less curvature and less helicity. (Taking the storm motion at a later time would result in a greater difference in the helicity between the large-curvature and

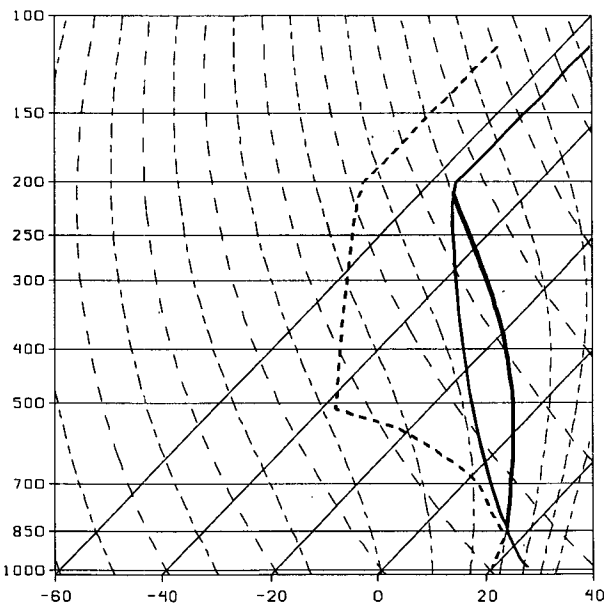

FIG. 1. Thermodynamic diagram for simulations. Mixing ratio at surface is 15 g kg^{-1}. Heavy line is pseudoadiabat associated with moist ascent of surface parcel.

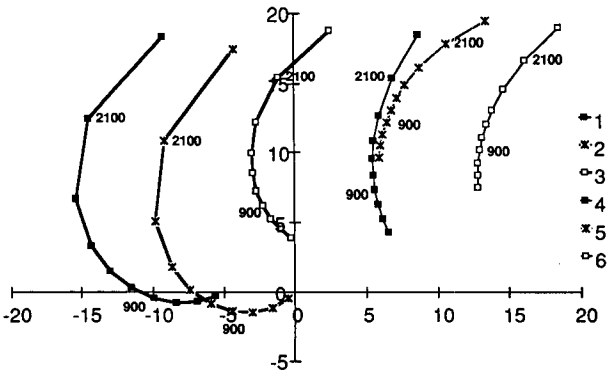

FIG. 2. Hodograph for lowest 3 km for simulations with curvature shear. Tick marks are 5 m s^{-1} apart. Hodographs offset for clarity. Points on the curves represent location of vertical levels. Heights are shown on the hodographs in meters.

TABLE 1. Parameters of the various hodographs. Low is the designation of the low-level hodograph as in Fig. 2, V_3 is the wind magnitude (m s^{-1}) at 3 km, dV is the change in wind magnitude from the ground to 3 km, dA is the change in wind direction (degrees of veering) from the ground to 3 km, Shear is the mean linear shear (10^{-3} s^{-1}) from the ground to 3 km, and A, B, and C are the bulk Richardson numbers for midlevel shear of 10×10^{-3} s^{-1} from 3 to 7 km, 5×10^{-3} s^{-1} from 3 to 7 km, and 5×10^{-3} s^{-1} from 3 to 11 km, respectively. The amount of helicity decreases in the hodographs as the numbers go from 1 to 6.

Low	V_3	dV	dA	Shear	A	B	C
1	15	10	180	11.0	26.5	28.3	28.3
2	20	20	140	11.0	27.6	29.7	29.7
3	15	10	105	7.0	26.8	34.2	34.2
4	20	15	40	5.9	29.2	37.4	37.4
5	15	5	65	5.0	26.7	39.6	39.6
6	20	10	45	5.2	28.1	39.5	39.5
Straight					7.6	30.2	30.2

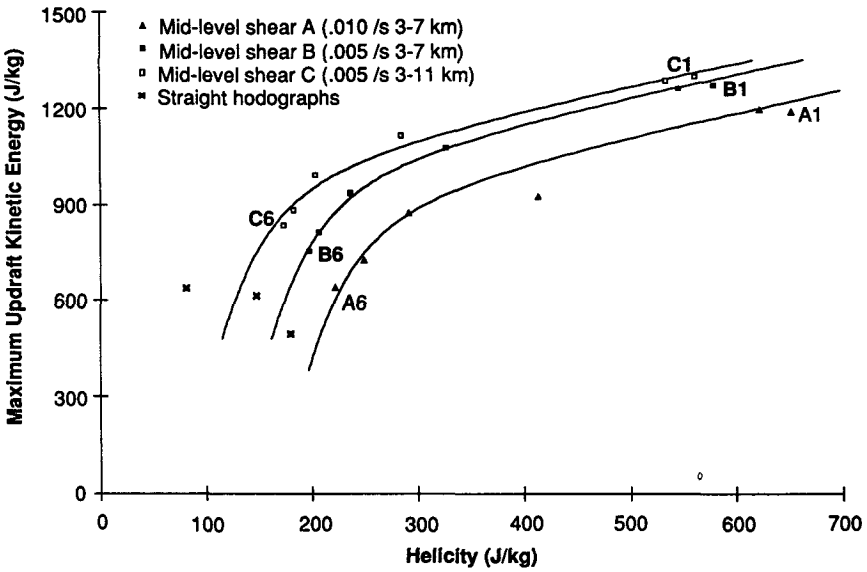

FIG. 3. Kinetic energy associated with maximum updraft ($w_{max}^2/2$) versus environmental helicity integrated over lowest 3 km. Hyperbola fitted by eye is shown for each of the three sets of mid-level shear cases with low-level curving hodographs.

small-curvature cases.) A section of a hyperbola is fitted by eye to each set of points associated with a curved hodograph at low levels and the same midlevel shear profile (A, B, or C in Table 1). The hyperbola is the same in each case and is merely shifted to best fit the points. With the exception of A3, the fit is quite good. Besides the increase in updraft intensity with helicity for a given midlevel shear, there is an increase in updraft intensity for a given low-level hodograph with decreasing midlevel shear. This apparently is due to the tendency of shear to suppress the growth of convective elements as discussed by Scorer and Ludlam (1953) and Lilly (1986a). The increase with helicity, however, is due to the organizing effects of shear, which have been described by Weisman and Klemp (1982, 1984). We stress that the effect is not simply an increase in the magnitude of the shear. The weakest updraft is associated with the straight hodograph with strong shear, which has approximately the same magnitude of shear as the strongly curved hodographs (A1 and A2). The strong relationship between the curvature of the hodograph and the updraft strength warrants closer examination to determine a possible cause–effect relationship.

To focus on the differences in updraft development, we will consider only the simulations with large and small amounts of curvature (A1 and A6, see Fig. 3) and having strong midlevel shear. The BRI of A1 and A6 are 26.5 and 28.2, respectively, while the helicities are 600 $m^2 s^{-2}$ (storm motion at this time $u = 4$ m s^{-1}, $v = 4$ m s^{-1}) and 300 $m^2 s^{-2}$ ($u = 4$ m s^{-1}, $v = 9$ m s^{-1}), respectively. The initial peak updrafts are 51.5 and 41.5 m s^{-1}. The time history of the maximum updrafts over the first 3600 s in these two simulations is shown in Fig. 4. Updraft A1 is initially slightly weaker but then becomes stronger after 1200 s. A weaker updraft in A1 is what one would expect from the Scorer and Ludlam (1953) argument. As time goes on in the simulations, the high-helicity updrafts tend to remain the strongest updrafts until the storms begin to decay.

In order to focus on the differences between the two developing storms, we will look at a time (1440 s), just after updraft A1 becomes stronger than updraft A6. Using the method of Weisman and Klemp (1984),

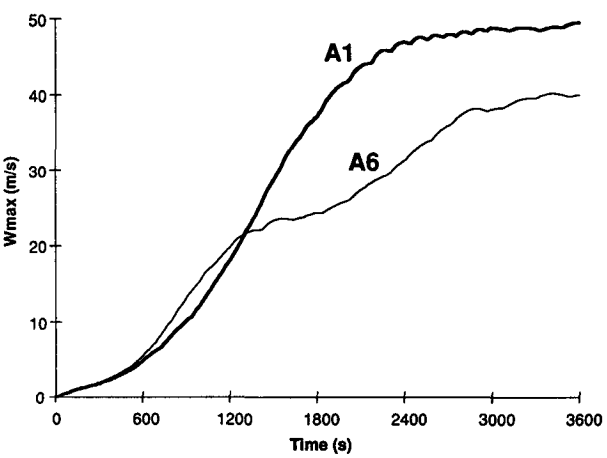

FIG. 4. Temporal evolution of w_{max} from large curvature (A1) (heavy line) and small curvature (A6) (light line) hodograph simulations.

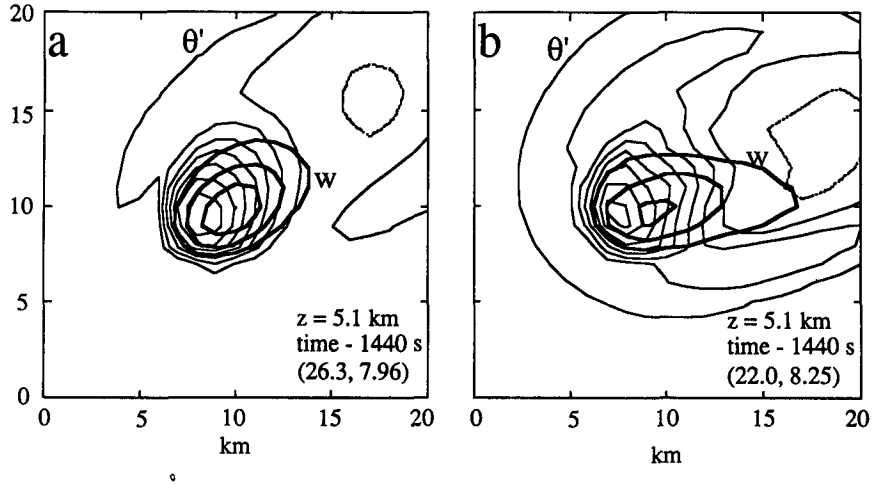

FIG. 5. Horizontal cross section of vertical velocity (heavy line) and perturbation potential temperature (light line) in 20 km × 20 km portion of domain at 5.1-km altitude at 1440 s in (a) large-curvature simulation (A1) and (b) small-curvature simulation (A6). Zero contour suppressed. Negative contours dashed. Contour interval for vertical velocity is 7 m s^{-1} and potential temperature is 1 K. Distance between tick marks is 5 km. The maximum vertical velocity and perturbation potential temperature are shown in parentheses in lower right corner of each panel.

vertical velocity and vorticity are well correlated in these updrafts by this time, indicative of supercellular structure. A horizontal cross section of vertical velocity and perturbation temperature at 5.1 km, the level of the peak updraft in both storms, is shown in Fig. 5. Note that the most unstable air is offset from the center of the updraft in both cases by 2–3 km. Displacement of the thermal and updraft maxima within thunderstorms has been seen in observations by Marwitz (1973). Also of interest is the fact that the maximum potential temperature perturbation is greater in A6, the weak updraft case (8.25 vs 7.96 K). The most unstable air does not correspond to the strongest updrafts because of the adverse vertical perturbation pressure gradient associated with the perturbation high pressure located on the west side of the updraft (Fig. 6).

The relationship between buoyancy and vertical pressure gradients can be seen more clearly by evaluating the accelerations acting on the rising parcels. For each of the two storms, we have constructed "pseudotrajectories" backwards from the location of the peak updraft and peak instability at 5.1 km and 1440 s. Model fields at 2-minute intervals were linearly interpolated to the 5-s time intervals used in computing the trajectories. Velocities at the trajectory locations are found by linearly interpolating in height between grid

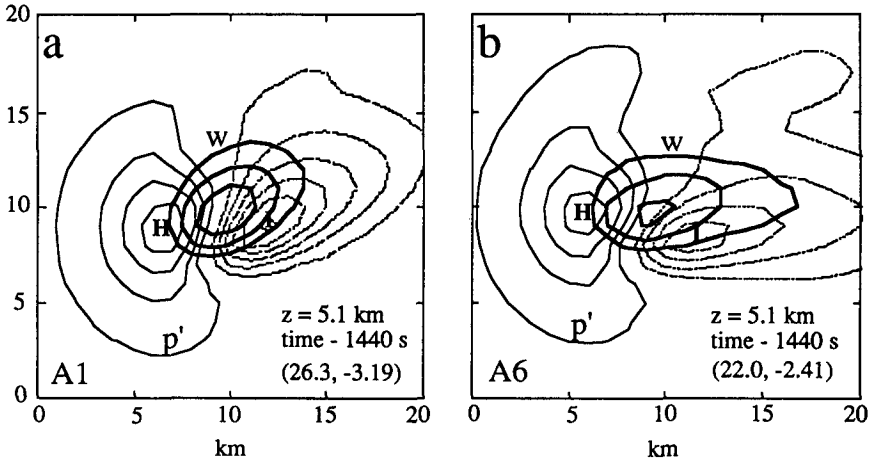

FIG. 6. Same as Fig. 5 except for vertical velocity and perturbation pressure (contour interval 0.5 hPa). The maximum vertical velocity and minimum perturbation pressure are shown in parentheses in lower right corner of each panel.

levels after bilinearly interpolating them in the horizontal at model levels. The pressure gradient between two levels at a given horizontal location is assumed constant for any height between those two levels. The buoyancy is calculated from the definition in (5). (Since changes from the base-state environmental potential temperature are no more than 0.2 K during the time period over which the trajectories are calculated, we have chosen to use the initial base state to compute the buoyancy for computational simplicity.)

The vertical velocity for the last 4 min along the trajectories is shown in Fig. 7. Accelerations of the thermal maxima parcels are small above 3.5 km, and the velocity difference between the thermal maxima and updraft maxima parcels increases rapidly above that height. Displaying the two acceleration terms for each of the parcels in the two storms reveals the physical processes leading to the differences (Fig. 8). The adverse vertical perturbation pressure force seen by the thermal parcels through most of their ascent is negative and cancels to a large extent the acceleration due to buoyancy particularly above 3.5 km. In contrast, for the updraft parcels, the acceleration due to pressure is not only positive but also greater than the buoyant acceleration below 3.5 km. Thus, the updraft at midlevels is fed by air that is initially weakly unstable, and is accelerated primarily by the perturbation pressure gradient in the early stages of its ascent. As it rises, it becomes warmer than its environment and the buoyant acceleration becomes more important. The importance of the acceleration due to the pressure gradient in the updraft maximum of supercells has been noted previously by Weisman and Klemp (1984).

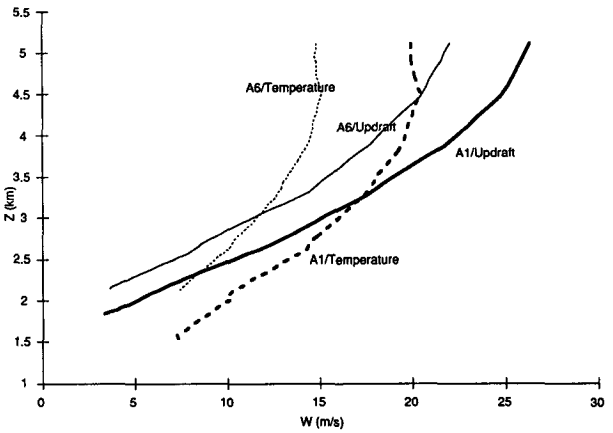

FIG. 7. Vertical velocity along pseudotrajectories calculated backward from vertical velocity and perturbation potential temperature maxima at 5.1 km at 1440 s. Heavy (light) lines associated with A1 (A6) storm. Solid (dashed) lines associated with vertical velocity (perturbation potential temperature) trajectories.

4. Vertical pressure gradient associated with a circular hodograph

Rotunno and Klemp (1982) theoretically considered the effects of shear on the vertical pressure gradient using a linearized model and also carried out a more extensive analysis using the full diagnostic pressure equation, requiring the solution of Poisson's equation for linear, nonlinear, and buoyancy terms. The simple relationship they derived from the linearized model was limited since that model implies that the region of low perturbation pressure is located downshear of the updraft. As Davies-Jones (1985) pointed out, this is not true except at midlevels of storms, with the departures becoming significant at low and high levels in the case of a circular hodograph. Since the pressure gradient acceleration seen in our results is at low levels, this is particularly important. McCaul (1989) developed a simple relationship for the effects of unidirectional shear on the vertical pressure gradient. We will derive a simple diagnostic relationship for the vertical pressure gradient acting on the flanks of an updraft in an environment with a *circular* hodograph. (Although none of the hodographs in the simulations was circular, this represents a limiting case. As such, it provides us with order of magnitude estimates of the effects of environmental hodograph curvature updrafts.) While both the work of McCaul and that presented here are consistent with the analysis using the full pressure equation by Rotunno and Klemp, we feel that these simple relationships have value in providing insight into the importance of hodograph shape without requiring extensive calculations.

To derive a relationship for a circular hodograph, we will use the results of Davies-Jones (1985), who derived an analytic relationship for the perturbation pressure for a simple model of a rotating thunderstorm in which motion in the storm is modeled as a Beltrami flow. Beltrami flows are characterized by the parallel relationship between the vorticity and velocity vectors (ω and $\mathbf{v}$, respectively) at each point in space, so that $\omega = \lambda \mathbf{v}$, where λ is a scalar constant. As such, they have many features in common with supercell thunderstorms, which are characterized by rotating updrafts. This similarity has been exploited theoretically in studies of supercell behavior (Lilly 1982, 1986b; Davies-Jones 1985).

Neglecting buoyancy, we start with the horizontal equation of motion, which can be written as

$$\frac{\partial \mathbf{v}}{\partial t} + \nabla\left(\frac{|\mathbf{v}|^2}{2}\right) - \mathbf{v} \times \omega = -\nabla \Pi, \qquad (8)$$

where ω is the three-dimensional vorticity and ∇ is the horizontal gradient operator. The Beltrami condition implies that the last term on the left side is zero. We further consider a dry, neutrally stratified, steady flow (so that the first term is zero) in a frame of reference moving with the storm. A flow configuration that meets the Beltrami restriction and resembles the gross features of an idealized thunderstorm updraft consists of radial

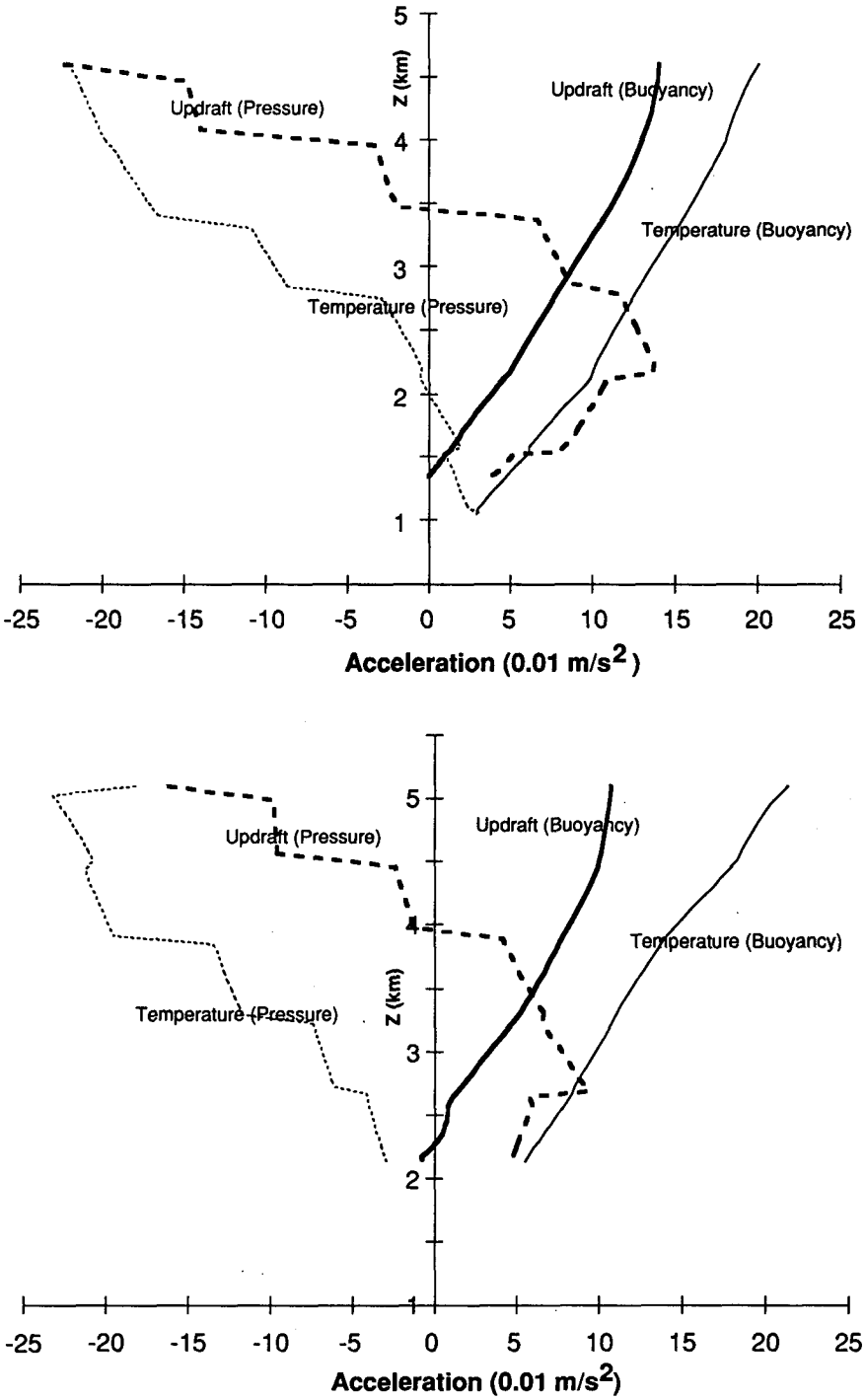

FIG. 8. Accelerations along trajectories of parcels discussed in Fig. 7. Heavy (light) lines associated with vertical velocity (perturbation potential temperature) maxima. Solid (dashed) lines associated with buoyancy (pressure gradient) force. (a) Large-curvature environment (A1). (b) Small-curvature environment (A6).

inflow at the surface into the updraft, with purely rotational flow at midlevels and radial outflow at the top of the updraft. For such a case, cylindrical coordinates are the natural choice for analysis. In cylindrical coordinates, a circular hodograph yields a mean flow such that

$$\bar{\mathbf{v}} = (-M\cos(\lambda z + \phi), M\sin(\lambda z + \phi), 0), \quad (9)$$

where M is the radius of the hodograph, where we have assumed that the storm motion is at the center of the hodograph, as was found in a numerical simulation with a circular hodograph by Lilly (1982). Lilly derived an expression for the vertical velocity in a Beltrami flow with a circular hodograph that can be written

$$w' = WJ_0(kr)\sin(\mu z) \quad (10)$$

with W as the maximum vertical velocity through the depth of the storm, J_0 is the order 0 Bessel function of the first kind, and $\mu = \pi/H$, where H is the height of the top of the updraft and

$$k = (\lambda^2 - \mu^2)^{1/2}. \quad (11)$$

The maximum updraft at any height is simply $W\sin(\mu z)$ at $r = 0$. The horizontal perturbation flow necessary to yield the Beltrami flow described above is given by the radial and tangential components, u' and v', as

$$u' = -\frac{\mu W}{k} J_1(kr)\cos(\mu z) \quad (12)$$

$$v' = \frac{\lambda W}{k} J_1(kr)\sin(\mu z). \quad (13)$$

Note that u' (the radial component) is inward at the surface ($z = 0$) and outward at the top of the storm ($z = H$) and v' (the tangential component) is zero at the surface and top of the storm and maximized at the middle of the storm, where the updraft is maximized.

Davies-Jones (1985) used the Bernoulli relationship to derive an analytic expression for the nondimensional perturbation pressure from (8), dividing it into a symmetric part and an asymmetric part. Since we are interested in the pressure gradient on the flanks of the storm, we will consider only the asymmetric contribution, Π'_A. Using the expressions for the flow components derived above, his result can be written as

$$\Pi'_A = \frac{MW}{k} J_1(kr)(\mu\cos(\lambda z + \phi)\cos(\mu z) + \lambda\sin(\lambda z + \phi)\sin(\mu z)). \quad (14)$$

Differentiating this with respect to z and combining terms gives

$$\frac{\partial}{\partial z}\Pi'_A = \frac{MW}{k} J_1(kr)(\lambda^2 - \mu^2) \times (\cos(\lambda z + \phi)\sin(\mu z)) \quad (15)$$

or

$$\frac{\partial}{\partial z}\Pi'_A = -MkWJ_1(kr)(\cos(\lambda z + \phi)\sin(\mu z)). \quad (16)$$

The cosine dependence in (16) means that the maximum perturbation pressure gradient will always be located on the upwind side of the updraft (see Fig. 2 of Davies-Jones 1985). While Davies-Jones considered only the location of the maximum value, we are interested in the magnitude. Solving (16) for the maximum value of the vertical pressure gradient at any height, which is located where $kr \approx 1.8$ and $\phi = -\lambda z$, yields

$$\max\left(\frac{\partial}{\partial z}\Pi'_A\right) = -0.58MkW\sin(\mu z). \quad (17)$$

A brief examination of the terms on the right-hand side of (17) reveals the physical meaning of the various terms. The 0.58 is the maximum value of J_1 (at $kr \approx 1.8$). The M and k describe the properties of the hodograph. As the magnitude of the storm-relative winds (M) and the rate at which wind direction (k) increase, the maximum pressure gradient also increases. [With $k = (\lambda^2 - \mu^2)^{1/2}$, a hodograph that turns 360° through the depth of the storm, $k = \sqrt{3}\mu$, while for a 720° turn, $k = \sqrt{15}\mu$.] The remainder of the right-hand side is simply the maximum updraft speed at height z.

The Beltrami constraints of no buoyancy, a circular hodograph, and updraft that depends on a sine function in the vertical limit the quantitative applicability of the model to storms. Significant qualitative insight can be gained, however, from looking at realistic values of the parameters in (16). Assuming a density of 1 kg m^{-3}, a hodograph with radius 10 m s^{-1} making a single revolution over the updraft depth of 12 km, and an initial updraft of 10 m s^{-1} yields a maximum acceleration of 0.026 m s^{-2} at 6 km. (A similar result can be obtained with from a scale analysis and is included as an Appendix.) For $\theta_0 = 300$ K, this acceleration is equivalent to a temperature excess of 0.8 K in buoyancy from (5). The acceleration at 2 km is half that, 0.013 m s^{-2}, equivalent to 0.4 K in buoyancy. Such an acceleration would be particularly significant at low levels where the buoyancy of a rising parcel typically is small. Given the presence of even a weak updraft at that height, the pressure gradient would accelerate air upward, helping it to lift low-level air to its level of free convection, above which it will become warmer than the environment. Thus, the presence of low-level curvature shear may enable the storm to tap the buoyancy of the environment.

While the Beltrami model applies strictly only to circular hodographs, the points it illustrates are important, and we would like to extend the results to more realistic hodographs. McCaul (1989, 1991) has shown examples of supercells in hurricane–tornado environments in which the low-level curvature is extreme and the buoyancy is low. In some cases, the storm-relative winds veer by a quarter circle over the lowest kilometer with an average magnitude of 10 m s^{-1}. If those parameters held through the depth of the atmosphere, they would be equivalent to having $k = \sqrt{35}\mu$ and $M = 10$ in (16). If we interpret the W

$\sin(\mu z)$ as the peak updraft at a given level, that would lead to an acceleration of 0.009 m s^{-2} (equivalent to a thermal perturbation of 0.3 K) for every 1 m s^{-1} of peak updraft. Thus, *if* some process, such as mechanical lifting, can initiate even a relatively weak updraft, the perturbation pressure gradient due to the curving hodograph can produce significant vertical accelerations, even in low buoyancy environments. The observation that supercells develop in low instability environments with hodographs containing strong low-level curvature may be related to this effect.

5. Discussion

The acceleration of an updraft at low levels due to shear has been previously noted by others (Rotunno and Klemp 1982; Weisman and Klemp 1984; McCaul 1989), but we want to emphasize the importance of curvature of the hodograph. Differences in the updraft intensity between the small- and large-curvature cases reach about 20%, and the curvature environment cases produce stronger updrafts than the straight hodograph cases. It is important to note that, except for the rectilinear shear cases, all of the hodographs showed significant amounts of curvature. Specifically, the intensification of the updraft in the large-curvature environment case results from a stronger upward-directed vertical perturbation pressure gradient. The presence of the stronger pressure gradient is consistent with the implications of the simple model using a circular hodograph and an idealized updraft. The simple model predicts increasing acceleration with increasing magnitude of the storm-relative wind (increasing radius of the hodograph), and increasing directional shear (increase in turning of the hodograph). We recognize the simplicity of the model shown here and only use it to deduce that pressure gradients in curving hodographs can be substantial. As with the simple model of Rotunno and Klemp (1982), the pressure gradient associated with the shear in the simple model cannot *initiate* an updraft (i.e., when $w = 0$ everywhere, there is no perturbation pressure gradient) but can *intensify* an already existing one produced by either a small amount or buoyancy or forced ascent. The qualitative predictions of the simple model, however, support the results of the numerical simulations in that the model storms with larger curvature hodographs have stronger updrafts than those with small curvature hodographs. Additional simulations with circular hodographs could be carried out to test this hypothesis more rigorously. Some of the simulations of Lazarus and Droegemeier (1990), which used sections of circles for the hodograph, are consistent with the results here. Most of the their simulations however, produced multicellular storms, so that comparison with the supercells simulated in this study is not possible for their entire dataset.

The vertical pressure gradient has important effects on the dynamics of the storm. It displaces the vertical velocity maximum from the buoyancy maximum at midlevels. The increase of the gradient with increasing curvature implies that the extreme low-level hodograph curvature frequently seen in tornadic storm environments may play an important role in intensifying the updraft in the storm. In particular, large curvature near the ground could serve to accelerate the buoyant air typically found at low levels to a height where that buoyancy can be released.

Acknowledgments. We thank Robert Davies-Jones, Chuck Doswell, and Don Burgess for their comments and suggestions. The comments of anonymous referees helped the arguments. In particular, we thank one of the referees for suggesting the scale analysis in the Appendix. This work was supported by NSF Grant ATM 87-00778. Computations were performed on the CRAY 2 at the National Center for Supercomputer Applications.

APPENDIX

Scale Analysis of Perturbation Pressure Gradient Associated with a Circular Hodograph

A result similar to (16) can be obtained by a scale analysis, beginning with (7). While in the Beltrami analysis we assumed that the flow was steady and $\mathbf{w} = \lambda\mathbf{v}$, here we assume that only the first and third terms in (7) are small compared to the others. Thus,

$$\nabla\left(\frac{|\mathbf{v}|^2}{2}\right) \sim -\nabla\Pi, \tag{A1}$$

so that

$$\frac{|\mathbf{v}|^2}{2} \sim -\Pi, \tag{A2}$$

and

$$\frac{\partial}{\partial z}\Pi \sim \frac{\partial}{\partial z}\left(\frac{|\mathbf{v}|^2}{2}\right). \tag{A3}$$

Now,

$$\frac{|\mathbf{v}|^2}{2} = \frac{M^2}{2} + M|\mathbf{v}'| + \frac{|\mathbf{v}'|^2}{2}. \tag{A4}$$

If we assume that the storm produces perturbation horizontal velocities on the order of the updraft velocities and that $|\mathbf{v}'|$ is on the order of or smaller than M, then we get that

$$\frac{\partial}{\partial z}\Pi \sim \frac{\partial}{\partial z}(Mw'). \tag{A5}$$

For an updraft in the form of a sine function, as in (9), we get that

$$\frac{\partial}{\partial z}\Pi \sim \mu MW = 0.026 \text{ m s}^{-2} \tag{A6}$$

for $M = W = 10$ m s^{-1}, as in the Beltrami analysis. The scale analysis requires looser assumptions on the magnitude of terms in Eq. (7) but is limited to a single revolution of the hodograph, so that it is more difficult to apply to cases with extreme low-level curvature such as those of McCaul (1989, 1991).

REFERENCES

Brooks, H. E., 1990: Low-level curvature shear and supercell thunderstorm behavior. Ph.D. thesis, University of Illinois, Urbana, IL, 233 pp. [Available from Department of Atmospheric Sciences, University of Illinois, 105 S. Gregory, Urbana, IL 61801.]

Davies-Jones, R. P., 1985: Dynamical interaction between an isolated convective cell and a veering environmental wind. Preprints, *14th Conf. on Severe Local Storms,* Indianapolis, Amer. Meteor. Soc., 216–219.

——, D. Burgess, and M. Foster, 1990: Test of helicity as a tornado forecast parameter. Preprints, *16th Conf. on Severe Local Storms,* Kananaskis Park, Alberta, Canada, Amer. Meteor. Soc., 588–592.

Klemp, J. B., and R. B. Wilhelmson, 1978: The simulation of three-dimensional convective storm dynamics. *J. Atmos. Sci.,* **35,** 1070–1096.

Lazarus, S. M., and K. K. Droegemeier, 1990: The influence of helicity on the stability and morphology of numerically simulated storms. Preprints, *16th Conf. on Severe Local Storms,* Kananaskis Park, Alberta, Canada, Amer. Meteor. Soc., 269–274.

Lilly, D., 1982: The development and maintenance of rotation in convective storms. *Topics in Atmospheric and Oceanographic Sciences: Intense Atmospheric Vortices,* L. Bengtsson and J. Lighthill, Eds., Springer-Verlag, 149–182.

———, 1986a: The structure, energetics, and propagation of rotating convective storms. Part I: Energy exchange with the mean flow. *J. Atmos. Sci.,* **43,** 113–125.

———, 1986b: The structure, energetics, and propagation of rotating convective storms. Part II: Helicity and storm stabilization. *J. Atmos. Sci.,* **43,** 126–140.

Marwitz, J. D., 1973: Trajectories within the weak echo regions of hailstorms. *J. Appl. Meteor.,* **12,** 1174–1182.

McCaul, E. W., Jr., 1989: The dynamics of simulated convective storms in hurricane environments. CIMMS Rep. No. 88. 185 pp. [Available from Cooperative Institute for Mesoscale Meteorological Studies, University of Oklahoma, 100 E. Boyd, Norman, OK 73019.]

———, 1991: Buoyancy and shear characteristics of hurricane–tornado environments. *Mon. Wea. Rev.,* **119,** 1954–1978.

Rotunno, R., and J. B. Klemp, 1982: The influence of the shear-induced pressure gradient on thunderstorm motion. *Mon. Wea. Rev.,* **110,** 136–151.

Scorer, R. S., and F. H. Ludlam, 1953: Bubble theory of penetrative convection. *Quart. J. Roy. Meteor. Soc.,* **79,** 94–103.

Weisman, M. L., and J. B. Klemp, 1982: The dependence of numerically simulated convective storms on vertical wind shear and buoyancy. *Mon. Wea. Rev.,* **110,** 504–520.

———, and ———, 1984: The structure and classification of numerically simulated convective storms in directionally varying wind shears. *Mon. Wea. Rev.,* **112,** 2479–2498.

Wilhelmson, R. B., and C. S. Chen, 1982: A simulation of the development of successive cells along a cold outflow boundary. *J. Atmos. Sci.,* **39,** 1466–1483.